Catalysis Today 146 (2009) 76–81

Contents lists available at ScienceDirect

Catalysis Today

journal homepage: www.elsevier.com/locate/cattod

Study on the steam reforming of ethanol over cobalt oxides

Chen-Bin Wang [a,*], Chia-Chan Lee [a], Jia-Lin Bi [a], Jia-Yi Siang [a], Jyong-Yue Liu [a], Chuin-Tih Yeh [b,c]

[a] Department of Applied Chemistry and Materials Science, Chung Cheng Institute of Technology, National Defense University, Tahsi, Taoyuan 33509, Taiwan, ROC
[b] Department of Chemical Engineering and Materials Science, Yuan Ze University Chungli, Taoyuan, Taiwan, ROC
[c] Fuel Cell Center, Yuan Ze University Chungli, Taoyuan, Taiwan, ROC

ARTICLE INFO

Article history:
Available online 20 January 2009

Keywords:
Cobalt oxides
Ethanol
Steam reforming

ABSTRACT

A high valence cobalt oxide, CoO_x, was prepared from a cobalt nitrate aqueous solution through precipitation with sodium hydroxide and oxidation by hydrogen peroxide. Furthermore, pure nanocrystalline cobaltic oxide (Co_3O_4) particles were obtained from the CoO_x by calcination at 300, 500 and 700 °C (labeled as C300, C500 and C700, respectively). All samples were characterized by X-ray diffraction (XRD), Raman spectroscopy and temperature-programmed reduction (TPR). Their catalytic activities toward steam reforming of ethanol (SRE) were tested in a fixed-bed reactor. The results showed that the phase components were transferred upon the treatment temperature, i.e., the CoO_x exhibited mainly CoO(OH), C300, C500 and the C700 exhibited Co_3O_4. The as-prepared CoO_x catalyst under low temperature possessed high activity. The best yield of hydrogen (Y_{H_2}) approached the theoretical value around 375 °C. Under H_2O/EtOH molar ratio of 13 and 22,000 h^{-1} gas hourly space velocity (GHSV) for the as-prepared CoO_x catalyst, the Y_{H_2} arrived 5.72 and only minor CO (<2%) and CH_4 (<0.8%) were detected.

1. Introduction

The current shortage of global energy and stringent emission regulations has stimulated interest in renewable energies. Fuel cells have been investigated as possible devices for direct conversion of the chemical energy of fuels (H_2 and O_2) into electrical energy that is able to provide clean and highly efficient electric power for both mobile and stationary applications [1]. The use of hydrogen as an energy carrier can support sustainable economic growth as well as reduce pollution and greenhouse gas emissions. From the environmental point of view the use of ethanol is preferred because renewable ethanol obtained from biomass offers high hydrogen content, non-toxicity, safe storage and easy handling [2–4]. The production of hydrogen from steam reforming of ethanol (SRE) could favor the use of hydrogen as an alternative fuel, addressing the difficulties of on-board hydrogen storage and distribution. Moreover, a high yield of hydrogen can be obtained from the SRE reaction [5–8]:

$$C_2H_5OH + 3H_2O \rightarrow 6H_2 + 2CO_2 \quad (1)$$

Our previous study discussed the supported and unsupported cobalt oxide in the oxidation of carbon monoxide [9–11]. In addition, the cobalt-based catalysts were considered as effective in steam reforming of ethanol [5,6,12–15]. In order to understand the role of active cobalt phases on SRE reaction, this study used X-ray diffraction (XRD), temperature programmed reduction (TPR) and Raman spectroscopy to characterize the cobalt oxides. Steam reforming of ethanol was performed using a water/ethanol to evaluate the capabilities of these materials to produce H_2 from a renewable and environmentally friendly fuel source. This study aimed to develop a highly efficient and more stable catalyst for the SRE using lower temperatures to generate H_2 with high selectivity and low CO in the outlet gas, which could facilitate relatively easier down-steam CO clean-up of PEMFC applications.

2. Experimental

2.1. Catalyst preparation

The as-prepared cobalt oxide (assigned as CoO_x) with a high valence state of cobalt was synthesized by the precipitation–oxidation method in an aqueous solution. The precipitation process was carried out at 50 °C, with 50 ml of 0.6 M $Co(NO_3)_2{\cdot}H_2O$ H_2O solution added drop by drop to 100 ml of 3.2 M NaOH solution; 100 ml of H_2O_2 (50 wt%) was then introduced dropwise under constant stirring. The precipitate was then filtered, washed with deionized water, and dried in an oven at 110 °C for 24 h. The

* Corresponding author.
E-mail addresses: chenbinwang@gmail.com, chenbin@ccit.edu.tw (C.-B. Wang).

0920-5861/$ – see front matter © 2009 Elsevier B.V. All rights reserved.
doi:10.1016/j.cattod.2008.12.010

dried CoO_x was further calcined under 300, 500 and 700 °C (labeled as C300, C500 and C700), respectively for 3 h.

2.2. Catalyst characterization

X-ray diffraction (XRD) measurements were performed using MAC Science MXP18 diffractometer with Cu $K_{\alpha 1}$ radiation (λ = 1.5405 Å) at 40 kV and 30 mA. The diffraction patterns were recorded in the 2θ value range of 10–80° with a step size of 0.01° and 1 s per step. The crystallite sizes of the cobalt oxides were estimated using the Scherrer equation.

The measurements of the Raman spectroscopy were recorded using a Nicolet Almega XR Dispersive Raman spectrometer. The spectra were collected between 150 and 2000 cm^{-1}, using the beam of a diode laser (780 nm), with the sample exposed to the air under ambient conditions.

Reduction behavior of cobalt oxides was studied by temperature-programmed reduction (TPR). Prior to testing, a sample of about 50 mg was preheated to 300 °C for degasification 1 h under N_2 flow (10 ml min^{-1}). After cooling to room temperature, a flow of 10% H_2/N_2 gas mixture was introduced at a flow rate of 10 ml min^{-1}. During TPR, the temperature was increased at 7 °C min^{-1} from room temperature to 600 °C.

2.3. Catalytic activity measurement

Catalytic activities of cobalt oxides toward SRE reaction were performed at atmospheric pressure in a fixed-bed flow reactor. A catalyst amount of 100 mg was placed in a 4 mm i.d. quartz tubular reactor, held by glass-wool plugs. The temperature of the reactor was controlled by a heating tape, and measured by a thermocouple (1.2 mm i.d.) at the center of the reactor bed. The feed of the reactants was comprised of a gaseous mixture of ethanol (EtOH), H_2O and Ar (purity 99.9995%, supplied by a mass flow controller). The composition of the reactant mixture (H_2O/EtOH/Ar = 37/3/60 vol.%) was controlled by a flow Ar stream (22 ml min^{-1}) through a saturator (maintained 120 °C) containing EtOH and H_2O. The gas hourly space velocity (GHSV) was maintained at 23,000 h^{-1} and H_2O/EtOH molar ratio was 13 (H_2O:EtOH = 80:20 by volume). Before the reaction, the sample was activated under air at 300 °C for 3 h. The SRE activity was tested stepwise, while increasing the temperature from 250 to 400 °C. A 5 h reaction time was maintained for each measured temperature.

The analysis of the reactants and all reaction products were carried out online by gas chromatography, with columns of Porapak Q and Molecular Sieve 5A for separation. Response factors for all products were obtained and the system was calibrated with appropriate standards before each catalytic test. The evaluation of SRE activity of all samples depends on the conversion of ethanol (X_{EtOH}), the distribution of products (mol%) and yield of hydrogen (Y_{H_2}). Both the X_{EtOH} and Y_{H_2} in the SRE reactions were calculated according to following equations:

$$X_{EtOH} = \frac{n_{EtOH\text{-}in} - n_{EtOH\text{-}out}}{n_{EtOH\text{-}in}} \times 100\,\% \quad (2)$$

$$Y_{H_2} = n_{H_2\text{-}out}/n_{EtOH\text{-}in} - n_{EtOH\text{-}out} \quad (3)$$

3. Results and discussion

3.1. Characterization of cobalt oxides

Fig. 1 shows the XRD profiles of cobalt oxides, which indicates that the as-prepared CoO_x [Fig. 1(a)] pattern matches the JCPDS 14-0673 file that identifies cobalt oxyhydroxide, CoO(OH), with a hexagonal structure (particle size around 10 nm) coupled with

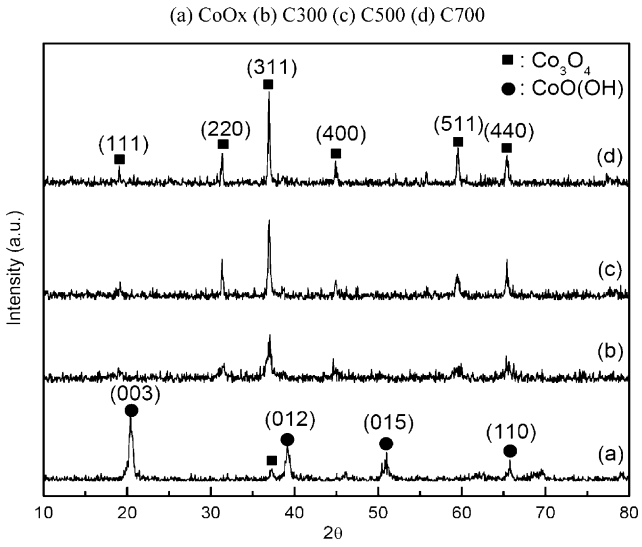

Fig. 1. XRD profiles of cobalt oxides: (a) CoO_x; (b) C300; (c) C500; (d) C700.

Co_3O_4. By increasing the calcined temperature, increasingly sharper peaks appear, whose positions and relative intensities are indicative of pure Co_3O_4 for C300, C500 and C700 samples [Fig. 1(b)–(d)]. Their mean particle size increase with the calcined temperatures, i.e., 13, 30 and 38 nm, respectively. Fig. 2 depicts the Raman spectra of the cobalt oxides. The as-prepared CoO_x sample shows bands at 298, 368, 482, 599 and 809 cm^{-1} [Fig. 2(a)], which are assigned as CoO(OH). Five Raman-active modes ($A_{1g} + E_g + 3\,F_{2g}$) are found in the C300, C500 and C700 samples [Fig. 2(b)–(d)]. The observed prominent Raman peaks correspond to the E_g (483 cm^{-1}), F_{2g} (524 and 619 cm^{-1}) and A_{1g} (690 cm^{-1}) modes of the Co_3O_4 crystalline phase and are in agreement with a previous report [15,16]. The band at 197 cm^{-1} is attributed to the characteristics of the tetrahedral sites, which is attributed to the F_{2g} symmetry [17]. These results further confirms that the transformation of CoO(OH) into Co_3O_4 is completed after calcinations above 300 °C. The structural distinctions can be found from the XRD and Raman spectrum.

Fig. 3 shows the TPR profiles of cobalt oxides. The as-prepared CoO_x [Fig. 3(a)] presents a continuous reductive step which occur at 219 (T_{r1}), 251 (T_{r2}), and 315 °C (T_{r3}), respectively. According to our previous paper [18,19], the CoO(OH) is initially reduced to Co_3O_4, and then subsequently reduced to CoO and Co metal. The

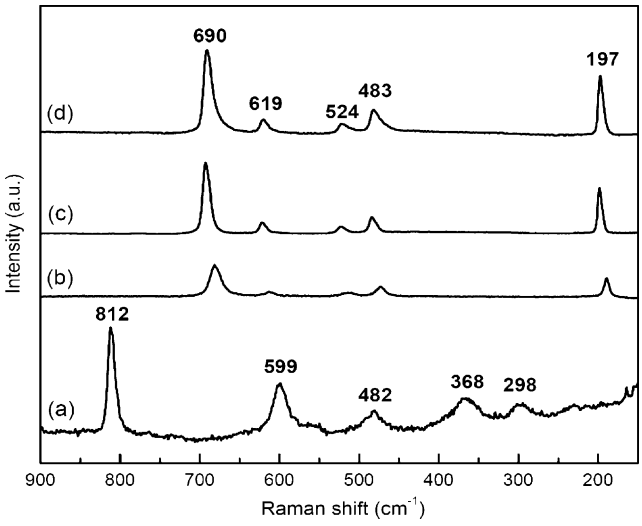

Fig. 2. Raman spectra of cobalt oxides: (a) CoO_x; (b) C300; (c) C500; (d) C700.

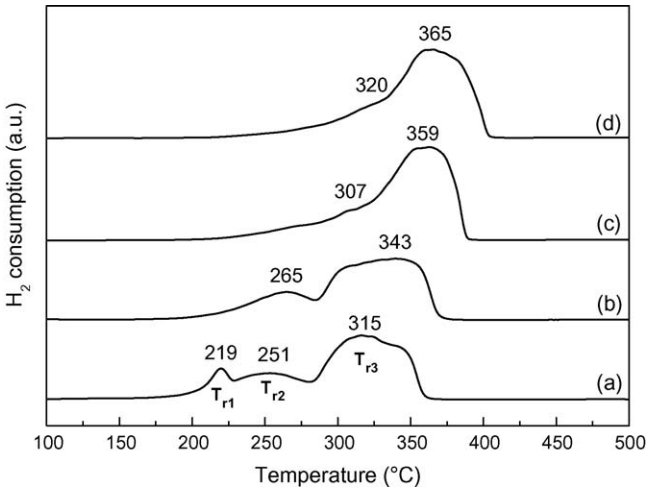

Fig. 3. TPR profiles of cobalt oxides: (a) CoO_x; (b) C300; (c) C500; (d) C700.

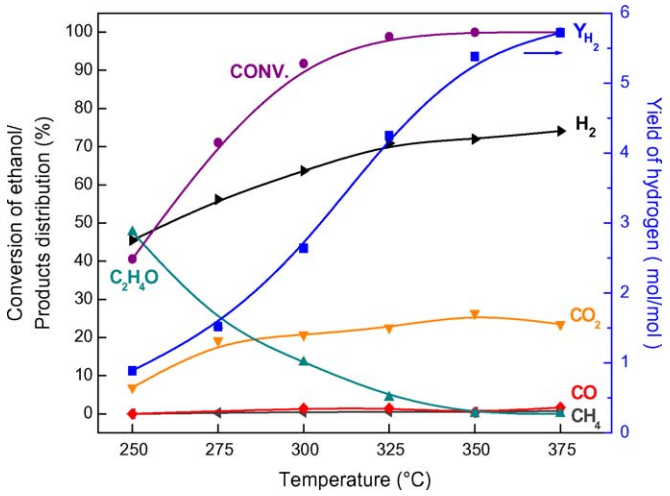

Fig. 4. Catalytic performance in the SRE reaction over CoO_x catalyst under H_2O/EtOH = 13 and GHSV = 22,000 h^{-1}.

profile points to a three-step reduction process:

$$CoO(OH) \xrightarrow{T_{r1}} Co_3O_4 \xrightarrow{T_{r2}} CoO \xrightarrow{T_{r3}} Co \quad (4)$$

The TPR profiles of the C300, C500 and C700 samples [Fig. 3(b)–(d)]. Fig. 3(b) shows only two reductive signals. Apparently, the reduction temperatures (T_{red}) shift to higher with the calcined temperatures and these phenomena originate from the agglomeration of cobalt oxides under pre-treatment conditions. According to literature [20–22], the low-temperature peak can be ascribed to the reduction of Co^{3+} ions into Co^{2+}, and the subsequent structural change to CoO. The high-temperature peak is attributed to the reduction of CoO to metallic cobalt. In comparison with as-prepared CoO_x, the disappearance of the peak around the lowest temperature indicates that the reductive behavior is in good agreement with the proposed Co_3O_4.

3.2. Catalytic performance on the SRE reaction

The SRE reaction is studied under a mixture of 3:37:60 of EtOH:H_2O:Ar (vol.%), between 250 and 400 °C, at atmospheric pressure. The catalytic performance of cobalt oxides, within in the steam reforming of the ethanol reaction at different temperatures (T_R), is compiled in Table 1 and Figs. 4 and 5, shown in terms of ethanol conversion and product distribution (water excluded) at each temperature. From the distribution of products (only H_2, CO_2, CH_3CHO, CO and CH_4) with different temperatures, some side-reactions are excluded in SRE: ethanol dehydration to ethylene [In the in situ FTIR analysis (not included in this paper) for SRE, we only observed the acetaldehyde and acetate species. Also, in the whole temperature ranges of reaction system do not measure the ethylene. So, we exclude the side-reaction]; ethanol decomposi-

Table 1
Catalytic performance of cobalt oxides in the steam reforming of ethanol.

Catalyst	T_R (°C)	t (h)	Conversion (%)	Products distribution (%)[a]					H_2/EtOH (mol/mol)	CO_2/EtOH (mol/mol)
				H_2	CH_4	CO	CO_2	C_2H_4O		
CoO_x	250	8	40.6	45.5	–	–	6.90	47.6	0.89	0.14
	275	14	71.1	56.2	0.25	–	19.2	23.2	1.52	0.53
	300	18	91.8	63.7	0.45	1.41	20.7	13.5	2.64	0.85
	325	24	98.8	70.9	0.57	1.45	22.6	4.30	4.25	1.36
	350	36	100	72.0	0.44	0.39	26.3	–	5.38	1.94
	375	48	100	74.1	0.75	1.67	23.4	–	5.72	1.81
C300	275	6	59.8	36.8	2.25	–	–	60.9	0.59	–
	300	10	77.6	55.9	0.31	1.28	24.8	17.5	1.82	0.81
	325	18	100	58.8	0.21	0.32	29.4	11.0	2.26	1.12
	350	24	100	69.9	0.37	1.36	28.3	–	4.66	1.88
	375	28	100	71.7	0.30	1.07	26.9	–	5.07	1.90
	400	30	100	73.9	0.57	2.04	23.4	–	5.68	1.80
C500	275	4	45.5	28.7	–	–	21.9	49.3	0.48	0.36
	300	8	60.8	51.8	0.07	–	18.8	29.2	1.34	0.48
	325	12	65.3	62.7	0.09	0.41	17.2	19.4	2.21	0.61
	350	16	75.6	68.9	0.39	1.86	23.5	5.27	3.80	1.29
	375	18	100	72.5	0.47	1.45	24.6	0.81	5.14	1.75
	400	20	100	73.7	0.42	1.42	24.4	–	5.62	1.86
C700	275	2	29.9	26.9	–	–	20.5	47.5	0.42	0.28
	300	4	42.2	34.6	0.07	–	18.9	45.7	0.62	0.35
	325	6	67.4	37.0	0.14	1.06	16.8	38.0	0.93	0.36
	350	8	92.1	44.6	0.22	2.07	16.3	29.7	1.31	0.43
	375	10	99.2	54.4	0.54	2.37	22.9	0.33	4.12	1.73
	400	12	100	69.4	0.79	2.29	27.4	–	4.55	1.79

C_2H_5OH:H_2O = 1:4 (v/v); GHSV = 22,000 h^{-1}.
[a] Water not included.

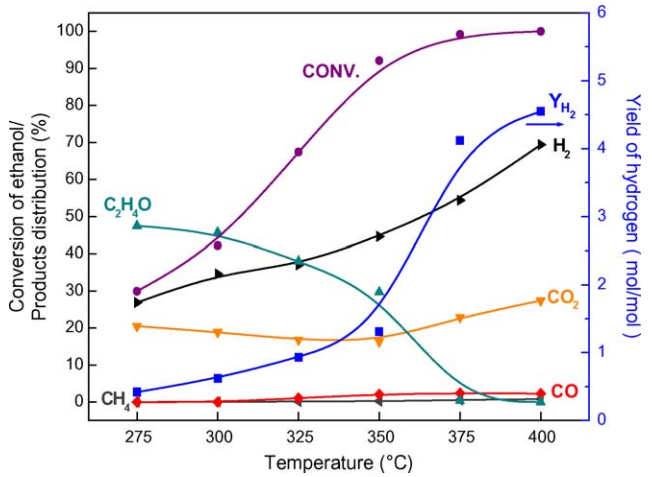

Fig. 5. Catalytic performance in the SRE reaction over C700 catalyst under H_2O/EtOH = 13 and GHSV = 22,000 h^{-1}.

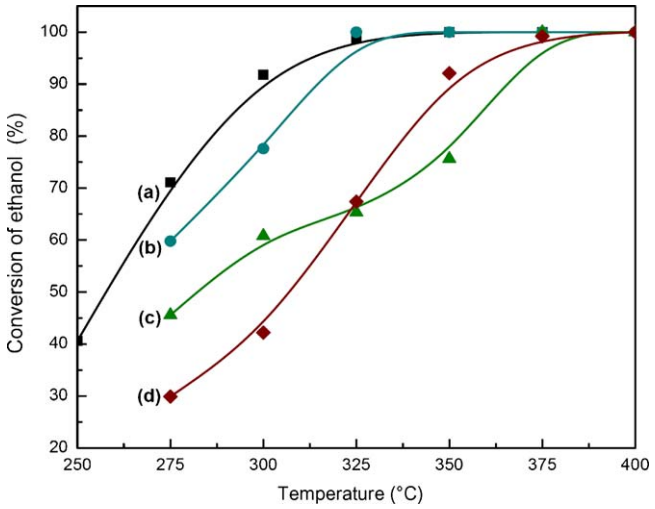

Fig. 6. Effects of reaction temperature for the ethanol conversion toward SRE reaction over cobalt oxides: (a) CoO_x; (b) C300; (c) C500; (d) C700.

tion to acetone; and ethanol decomposition to CO, CH_4 and H_2 (since only minor CO and CH_4 at all temperature ranges).

Ethanol conversion and H_2 production increase with T_R for all samples. Under high conversion distribution, high selectivity to H_2 and CO_2 (see last two columns of Table 1) are achieved (near the stoichiometric values for the SRE reaction). Complete conversion arrives around 325 °C for CoO_x and C300 samples, while, around 375 °C for C500 and C700 samples. Comparison of these results and the references reported [5,6,12–15], except for Homs and co-workers [15] discussed the Co_3O_4 catalyst, while others discussed the supported cobalt catalysts. Among these catalysts, the best catalyst was obtained by Homs et al. under $T_R = 400$ °C ($S_{H_2} = 73.3, Y_{H_2} = 5.49$). In this study, the high valence CoO_x acquired better activity ($T_R = 375$ °C, $S_{H_2} = 74.1, Y_{H_2} = 5.72$) for SRE reaction. This may suggest that the as-prepared cobalt oxide possesses a high valence and small size of particle. The lower temperature (<325 °C) presents large amounts of CH_3CHO and decreasing amounts of CH_3CHO, that accompany the increasing H_2 with T_R. Apparently, the dehydrogenation of ethanol to acetaldehyde is the first step with cobalt oxides.

$$C_2H_5OH \rightarrow CH_3CHO_{(a)} + H_2 \quad (5)$$

The acetaldehyde can be transformed in different pathways: decomposes to methane and carbon monoxide or on the surface of cobalt oxide it can be oxidized to acetate and follow decomposes into methyl group and CO_2

$$CH_3CHO_{(a)} \rightarrow CH_4 + CO \quad (6)$$

$$CH_3CHO_{(a)} \xrightarrow{[O]} CH_3COO_{(a)} \quad (7)$$

$$CH_3COO_{(a)} \rightarrow CH_{3(a)} + CO_2 \quad (8)$$

In addition, the methyl group can further react with surface OH species or water to form carbon monoxide and hydrogen [23]

$$CH_{3(a)} + OH_{(a)} \rightarrow CO + 2H_2 \quad (9)$$

$$2CH_{3(a)} + 2H_2O \rightarrow 2CO + 5H_2 \quad (10)$$

In the presence of water, the side-reactions of water gas shift (WGS) reactions, and steam reforming of methane may also occur

$$CO + H_2O \rightarrow CO_2 + H_2 \quad (11)$$

$$CH_4 + H_2O \rightarrow CO + 3H_2 \quad (12)$$

Due to the endothermic nature of steam reform of methane ($\Delta H_r = 206$ kJ/mol), the reaction (12) is carried out at high temperatures (around 600–900 °C) to achieve high conversion rates [24–28]. From the minor distribution of CO and CH_4 between 250 and 400 °C for cobalt oxides (see Table 1), pathways of (9) and (10) are plausible. Accompanied the WGS reaction with CO oxidation on cobalt oxides [9–11] derive the minor CO distribution.

Figs. 6 and 7 summarize the effects of temperature on X_{EtOH} and Y_{H_2} of cobalt oxides. The results confirm that the activity of as-prepared CoO_x and C300 are better than C500 and C700, with both a lower T_R and a higher Y_{H_2} for the CoO_x and C300, which can be expressed as a connection between catalytic activity and crystallite size. The catalytic activity decreases with increasing particle size. Under H_2O/EtOH molar ratio of 13 and 23,000 h^{-1} GHSV for as-prepared CoO_x catalyst, the Y_{H_2} arrives 5.38 under 350 °C and only minor CO (<0.5%) and CH_4 (<0.5%) are detected, while for the C300 sample, the Y_{H_2} arrives 4.66 under 350 °C, and minor CO (<2%) and CH_4 (<0.5%) are detected. This can express that there is a connection between catalytic activity and phases of cobalt oxide as the high valence cobalt oxide acquires the higher catalytic activity. Otherwise, the factor to enhance the activity also depends on the cleavage temperature of the C–C bond (T_d). Comparison of

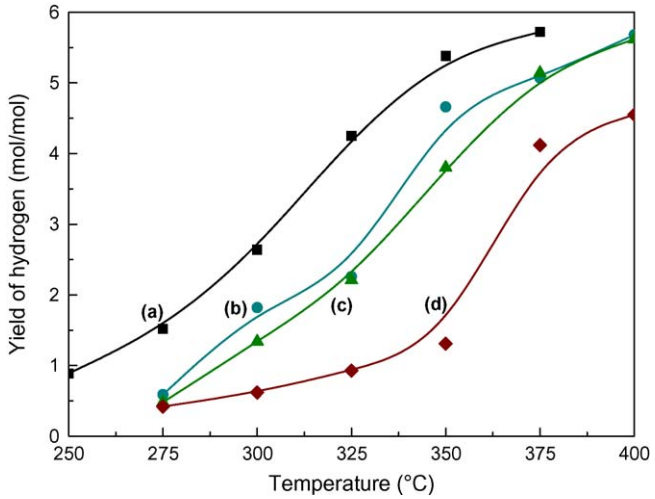

Fig. 7. Effects of reaction temperature for the yield of hydrogen toward SRE reaction over cobalt oxides: (a) CoO_x; (b) C300; (c) C500; (d) C700.

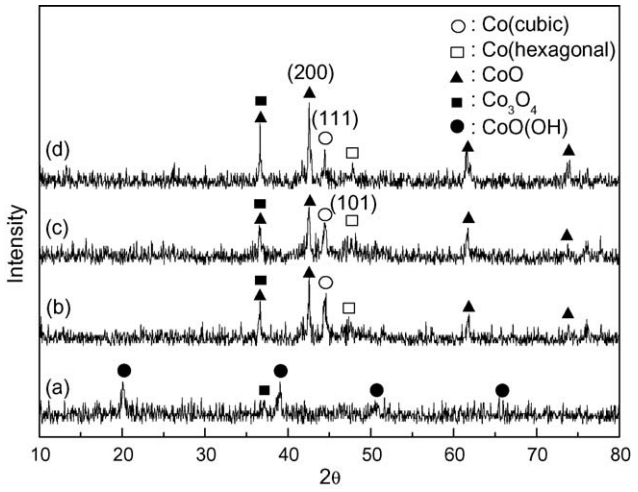

Fig. 8. XRD profiles of cobalt oxides after SRE reaction: (a) CoO_x; (b) C300; (c) C500; (d) C700.

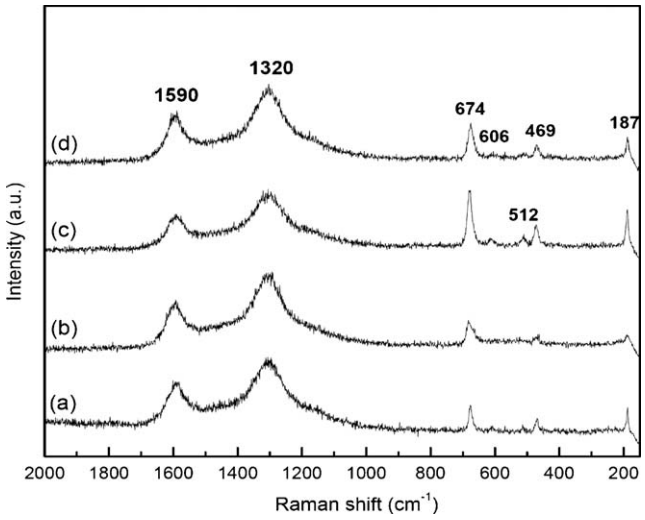

Fig. 9. Raman spectra of cobalt oxides after SRE reaction: (a) CoO_x; (b) C300; (c) C500; (d) C700.

the distribution of acetaldehyde, under different temperatures of the four samples, shows the T_d around 300 °C for CoO_x, 325 °C for C300 and C500, 350 °C for C700 sample, respectively.

3.3. Characterization of used catalysts

Although the catalytic performance of SRE is excellent over cobalt oxides, catalytic behavior at 375 °C is maintained for 2 days for CoO_x; 1 day for C300 and C500 at 400 °C; and half day for the C700 sample at 400 °C, respectively. Longer reaction periods produce a progressive deactivation of the activity, which may be the carbon deposition or the phase transformation of the cobalt oxides under steam reforming condition. In order to obtain more information about the behavior of deactivation, characterization of XRD, Raman and TPR were pursued for samples after the SRE catalytic tests.

Fig. 8 shows the XRD profiles of cobalt oxides after SRE reaction (at 375 °C maintained 2 days for CoO_x; 1 day for C300 and C500 at 400 °C; 1/2 day for C700 sample at 400 °C). With the exception of the CoO_x sample, the phase compositions of other samples are transferred into multiple phases. Compared used CoO_x [Fig. 8(a)] with fresh sample [Fig. 1(a)], CoO(OH) is coupled with a little Co_3O_4 phase. While the XRD patterns of C300, C500 and C700 samples [Fig. 8(b)–(d)] after SRE reaction are changed. Aside from the (3 1 1) plane of Co_3O_4, which overlapped with the (1 1 1) plane of CoO at around $2\theta = 36.8^\circ$, the XRD pattern exhibited diffraction lines corresponding to metallic cobalt [including the (1 1 1) plane of cubic β-Co at $2\theta = 44.3^\circ$ and (1 0 1) plane of hexagonal α-Co at $2\theta = 47.3^\circ$] and CoO. With the exception of the Co_3O_4 species, particle size of the other species can be calculated. Table 2 summarizes the phase composition and particle size of fresh and used cobalt oxides measured from XRD data. It is found that the particle size does not show an apparent increase after the SRE reaction. Thermal stability for the as-prepared CoO_x only exists on the CoO(OH) and Co_3O_4 species after the SRE reaction shows less deactivation. Perhaps the phase transformation of cobalt oxide in the SRE condition is one cause of the easy deactivation of C300, C500 and C700 samples.

Table 2
Phase composition and particle size of fresh and used cobalt oxides[a].

Catalyst	Fresh		Used	
	Composition	*d* (nm)	Composition	*d* (nm)
CoO_x	CoO(OH)	10	CoO(OH), Co_3O_4	7, 8
C300	Co_3O_4	13	Co_3O_4, CoO, Co[b], Co[c]	–, 13, 14, 12
C500	Co_3O_4	30	Co_3O_4, CoO, Co[b], Co[c]	–, 16, 12, 11
C700	Co_3O_4	38	Co_3O_4, CoO, Co[b], Co[c]	–, 18, 11, 10

[a] Measured and calculated from XRD data.
[b] Co (cubic).
[c] Co (hexagonal).

The Raman spectra (Fig. 9) of cobalt oxides after SRE reaction differ from those of fresh samples (Fig. 2). Two Raman regions can be distinguished between fresh and used samples. One region for cobalt oxides (180–1000 cm^{-1}), the Raman spectra show the bands at 187, 469, 512, 606 and 674 cm^{-1}. These bands are low-intensity, broad, and at lower wave numbers than those seen with Co_3O_4 [Fig. 2(b)–(d)], which is attributed to the reduction of most of the Co_3O_4 into metallic cobalt and CoO. Other regions for carbon deposition (1100–1800 cm^{-1}), show the absence of carbon deposits on the fresh samples. While the Raman spectra of used samples show two bands centered at 1320 and 1590 cm^{-1}, which are characteristic of poorly ordered carbon deposition [29]. In the SRE reaction, not ethylene and acetone products are observed, thus, the carbon deposition on the used catalysts may result from the Boudouard reaction [6]:

$$2CO \rightarrow CO_2 + C \quad (13)$$

The evidence of the carbon deposition also can be demonstrated by TPR. Fig. 10 shows the TPR profiles of cobalt oxides after SRE reaction, which are the same as the Raman spectra, two reduced

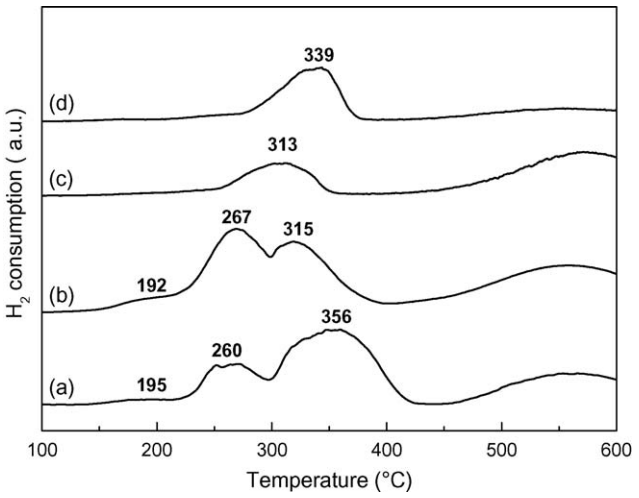

Fig. 10. TPR profiles of cobalt oxides after SRE reaction: (a) CoO_x; (b) C300; (c) C500; (d) C700.

regions can be distinguished between the fresh and used samples. One region of cobalt oxides (150–450 °C), the used CoO_x [Fig. 10(a)], presents similar reduction behavior with the fresh sample. The reduction behavior of used C300 samples [Fig. 10(b)] presents Co_3O_4 and CoO, while other reduction behavior of the used samples [Fig. 10(c) and (d)] show only CoO. Other regions of carbon deposition (450–600 °C) shows that the broad signal comes from the methanation of deposited carbon [5]:

$$C + 2H_2 \rightarrow CH_4 \quad (14)$$

According to the characterization, it can be concluded that both the carbon deposition and phase transformation of cobalt oxides may be the reasons for the deactivation of reforming catalysts.

4. Conclusion

An excellent ethanol reforming catalysts was developed in this study. The as-prepared CoO_x catalyst under low temperature possessed high activity. The best Y_{H_2} approached the theoretical value around 375 °C. Under an EtOH/H_2O molar ratio of 1/13 and 22,000 h^{-1} GHSV for the as-prepared CoO_x catalyst, the Y_{H_2} arrived 5.72 and only minor CO (<2%) and CH_4 (<0.8%) were detected.

Acknowledgement

We are pleased to acknowledge the financial support for this study by the National Science Council of the Republic of China under contract number NSC 96-2113-M-606-001-MY3.

References

[1] M.C. Batista, R.K.S. Santos, E.M. Assaf, J.M. Assaf, E.A. Ticianelli, J. Power Sources 134 (2004) 27.
[2] D.K. Liguras, D.I. Kondarides, X.E. Verykios, Appl. Catal. B 43 (2003) 345.
[3] G. Maggio, S. Freni, S. Cavallaro, J. Power Sources 74 (2001) 17.
[4] L.F. Brown, Int. J. Hydrogen Energy 26 (2001) 381.
[5] J. Llorca, N. Homs, J. Sales, P. Ramirez de la Piscina, J. Catal. 209 (2002) 306.
[6] A. Haryanto, S. Fernando, N. Murali, S. Adhikari, Energy Fuels 19 (2005) 2098.
[7] P.D. Vaidya, A.E. Rodrigues, Chem. Eng. J 117 (2006) 39.
[8] P.K. Cheekatamarla, C.M. Finnerty, J. Power Sources 160 (2006) 490.
[9] C.B. Wang, H.C. Tsai, C.W. Tang, S.H. Chien, Catal. Lett. 107 (2006) 223.
[10] C.B. Wang, C.W. Tang, H.C. Tsai, M.C. Kuo, S.H. Chien, Catal. Lett. 107 (2006) 31.
[11] C.W. Tang, C.C. Kuo, M.C. Kuo, C.B. Wang, S.H. Chien, Appl. Catal. A 309 (2006) 37.
[12] F. Haga, T. Nakajima, H. Miya, S. Mishima, Catal. Lett. 48 (1997) 223.
[13] J. Llorca, P. Ramirez de la Piscina, J.A. Dalmon, J. Sales, N. Homs, Appl. Catal. B 43 (2003) 355.
[14] J. Llorca, N. Homs, J. Sales, J.L.G. Fierro, P. Ramirez de la Piscina, J. Catal. 222 (2004) 470.
[15] J. Llorca, P.R. Piscina, J.A. Dalmon, N. Homs, Chem. Mater. 16 (2004) 3573.
[16] V.G. Hadjiev, M.N. Iliev, I.V. Vergilov, J. Phys. C: Solid State Phys. 21 (1988) L199.
[17] C.V. Ramana, M. Massot, C.M. Julien, Surf. Interface Anal. 37 (2005) 412.
[18] H.K. Lin, H.C. Chiu, H.C. Tsai, S.H. Chien, C.B. Wang, Catal. Lett. 88 (2003) 169.
[19] C.B. Wang, H.K. Lin, C.W. Tang, Catal. Lett. 94 (2004) 69.
[20] C.B. Wang, C.W. Tang, S.J. Gau, S.H. Chien, Catal. Lett. 101 (2005) 59.
[21] P. Arnoldy, J.A. Moulijn, J. Catal. 93 (1985) 38.
[22] M. Vob, D. Borgmann, G. Wedler, J. Catal. 212 (2002) 10.
[23] M. Domok, M. Toth, J. Rasko, A. Erdohelyi, Appl. Catal. B 69 (2007) 262.
[24] A.A. Lemonidou, M.A. Goula, I.A. Vasalos, Catal. Today 46 (1987) 175.
[25] M. Mamak, N. Coombs, G. Ozin, Adv. Mater. 12 (2000) 198.
[26] P. Bera, S. Mitra, S. Sampath, M.S. Hegde, Chem. Commun. (2001) 927.
[27] T. Takeguchi, S.N. Furukawa, M. Inoue, J. Catal. 202 (2001) 14.
[28] X. Wang, R.J. Gorte, Appl. Catal. A 224 (2002) 209.
[29] P. Lespade, A. Marchand, M. Couzi, F. Cruege, Carbon 22 (1984) 375.